Carbon nanostructures grown with electron and ion beam methods.

P. Lemoine , SS Roy , PD Maguire and JAD McLaughlin

Northern Ireland Bioengineering Centre- Nanotechnology Research Institute, University of Ulster at Jordanstown, Northern Ireland, United Kingdom

ABSTRACT

We present a comparative study where carbon nanostructures were prepared by electron and ion beam methods. The deposited thin films were analysed by Raman analysis, nanoindentation, Energy dispersive X-ray analysis (EDX) and atomic force microscopy (AFM). In most conditions, the material formed is hydrogenated amorphous carbon. This study was used to form sharp AFM supertip structures which were successfully used to image sintered ceramic samples.

Keywords: hydrogenated amorphous carbon, focused ion beam, electron beam induced deposition, nanoindentation, Raman spectroscopy

1 INTRODUCTION

The structuring and etching of carbon materials is essential for a number of applications which include field emission displays, micro-mechanical systems and data storage components.[1] The traditional method is to sequentially deposit and pattern the various components of the device. The difficulty is that both tasks often use energetic ions and electrons. For instance, diamond-like carbon (DLC), mostly prepared by plasma deposition techniques, is formed by the bombardment of energetic ionic species. Carbon nanotubes (CNT), often prepared by Chemical Vapour Deposition methods, are also growing from an environment of intense ionic bombardment. It seems, therefore, that, an optimised deposition process could well result in a pattern of transformed material with inadequate properties. For carbon, the main problem is graphitisation which is known to occur, in Diamond-like carbon (DLC) for instance, following intense visible[2] or ionic irradiation.[3] Ion beams are also used for doping CNT and, likewise have the potential to create defects on the surface of the CNT. Another problem with this dual deposition/patterning approach is the complexity and cost of the systems, which cannot always be justified, in a commercial context. The alternative strategy discussed here is to use a single step process to simultaneously deposit and pattern the device. Its added advantage is that three-dimensional structures can easily be built by this method and, in theory, process parameters (current density, kV, pressure, etc.) can be tuned more independently than in conventional plasma deposition systems.

The idea behind this technology is that hydrocarbon layers often built up on material surfaces when subjected to electron or ion beam irradiation in the presence of oil vapours from the vacuum system. Electron microscopists have always endeavoured to remove these contamination layers and observe the pristine surface below. However, over the last twenty years, there has been some effort to use this process as a writing tool for device fabrications.[4] This method has produced single electron transistors, AFM supertips and tough nm thick resist for the electrochemical formation of porous silicon.[5,6,7] In a preliminary study, we compared results obtained with a conventional Scanning electron microscope (SEM) and a Focused ion beam (FIB) system equipped with a naphthalene gas injector.[8] The work presented here discuss carbon films prepared using the same FIB-SEM dual system.

2 EXPERIMENTALS

We used a Quanta 3D FEI dual FIB/SEM system. The base pressure was 10^{-6} torr and the carbon was grown from a naphthalene gas injector over 10x10 μm^2 areas, using the patterning software of the instrument. The films were grown on Si wafers placed at the coincidence point of the two beams, corresponding to a 15mm SEM working distance. The electron beam deposited (EBD) carbon structures were prepared at 1, 2 and 5kV with current varying from 1.3nA to 1.6nA. The ion beam deposited (IBD) carbon structures were grown accelerating the ion beam at 30kV with Gallium ion currents varying from 30 pA to 7nA. The exposure time was fixed to give the same film thickness for all samples, according to the instrument's patterning software. The resulting approximate charges doses were 10^{-8} C/μm^2 and 10^{-9} C/μm^2 for the EBD and IBD experiments, respectively. The roughness and thickness of these carbon nanostructures were analysed with a Dimension 3100 AFM microscope operating either in tapping mode or contact mode. In addition, lateral force microscopy (LFM) images were also acquired. The Raman spectra were obtained with HeNe laser excitation (633nm) using a Labram confocal Raman microscope. The hardness (H) and Young modulus (E) of the samples were measured with a MTS nanoindenter XP®, using the dynamical contact module in continuous stiffness measurements mode. These indentations were carried out at a constant strain rate of $0.05s^{-1}$ up to a depth of 300nm. The tip area function was calibrated using fused silica and the data were analysed using the Oliver and Pharr method.[9] The EDX spectra were obtained using an Oxford Instrument spectrometer coupled to a Hitachi S3200N SEM microscope operated at 5kV, to maximize surface sensitivity. The elements C, O, Si and Ga were calibrated, respectively with graphite, quartz, Si and

GaAs standard spectra acquired also at 5kV. The quantification and calibration of the spectra were done using the Si wafer and a ZAF protocol.

3 RESULTS

Figure 1 and 2 shows the growth rate of the EBD and IBD samples, as a function of deposition parameters. The EBD growth rate decreases with SEM accelerating voltage whereas the IBD growth rate increases with the FIB current. Moreover the EBD growth rates are much smaller than the IBD ones.

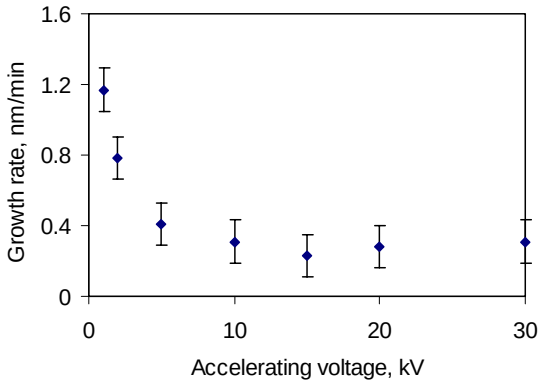

Figure 1: Growth rate for the EBD carbon films

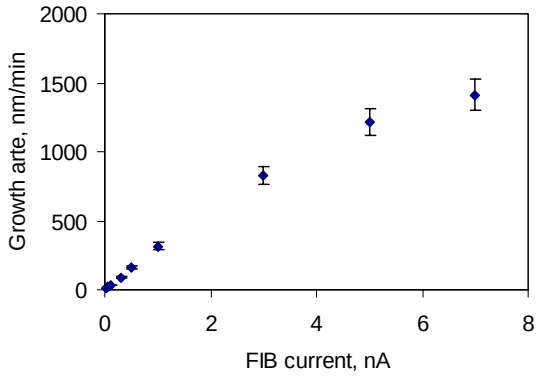

Figure 2: Growth rate for the IBD carbon films

The roughness R_a values of the EBD and IBD samples are, respectively 0.6±0.2nm and 3±1nm. The EBD and IBD film's thickness vary, respectively from 13nm to 35nm and from 350nm to 650nm. This indicates that the patterning software of the instrument is not accurately calibrated against growth rate. Figure 3 shows LFM images acquired at a 90 degree scan angle with a 0.06N/m Si_3N_4 contact AFM probe for a milled Si area, at 0.1nA and for an IBD carbon area also prepared at 0.1nA. The friction signal is clearly noticeable and significantly larger than the noise signal due to cross-talk between the bending and torsion signals of the AFM photodetector. This friction contrast with respect to the unexposed area is –0.11V±0.01V and 0.083V±0.01V, respectively for the milled Si and IBD films. Therefore, if the FIB irradiation reduces the friction of the AFM tip on the Si substrate, it tends to increase the friction on the IBD carbon films. Moreover, we found that the friction signal does not vary significantly with the FIB current.

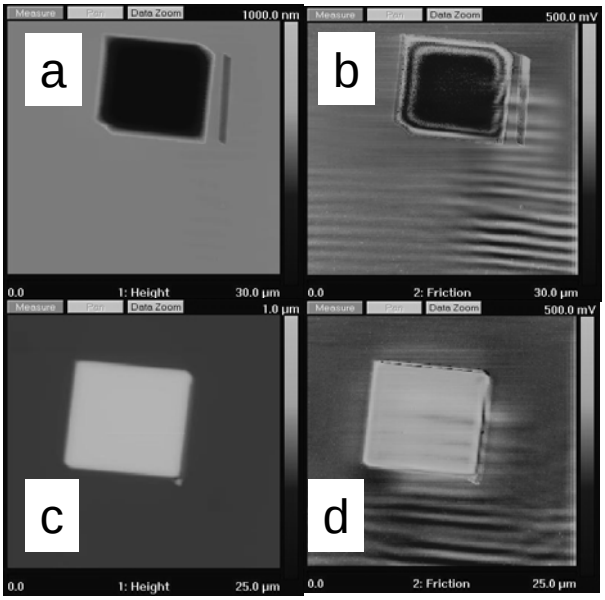

Figure 3: LFM images of patterned 10x10 μm^2 areas; height (a) and friction contrast (b) for a milled Si at 0.1 nA and height (c) and friction contrast (d) for a IBD carbon film at 0.1nA.

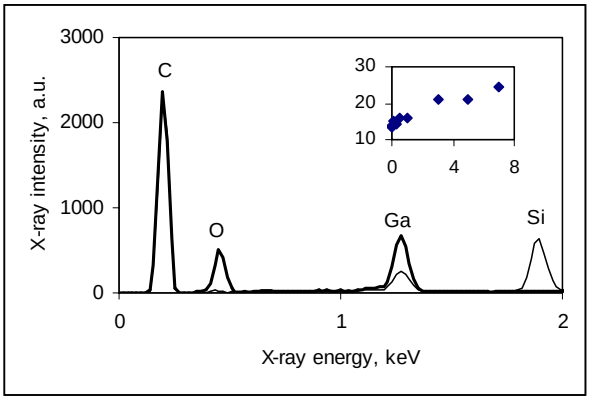

Figure 4: EDX spectra of an IBD film, prepared at 7nA and a milled Si surface. The insert shows the Ga at.% of the various IBD films versus FIB current, in nA.

Some EDX spectra are shown in figure 4. After quantification, the EDX analysis of the IBD samples shows that these films contain mainly C and Ga, with minute quantities of O and Si, possibly originating from the substrate. The Ga atomic percentage, plotted in the insert of figure 4, increases with the FIB current.

Figure 5 and 6 display the Raman spectra of these EBD and IBD films. Both set of spectra show the broad asymmetric features indicative of amorphous carbon. These were deconvoluted into the usual G and D peaks, respectively around 1350 cm^{-1} and 1550 cm^{-1}. The resulting G peak position and intensity ratio I_D/I_G are presented in figure 7 for the IBD samples.

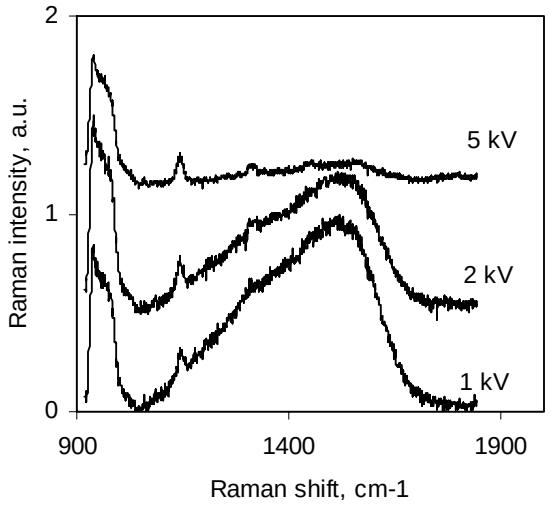

Figure 5: Raman spectra of the EBD samples

AFM microscopy was used to locate the indents and insure that only those indents positioned on the EBD and IBD 10x10 μm^2 patterns were considered. In figure 8, we report the E and H values of the IBD samples, calculated at 10% of the film thickness (t/10). Although this protocol is not always valid, as the response of a coated system is influenced by the mechanical properties of the substrate[10], we expect it to be adequate in this case as the film and substrate have similar properties and the t/10 depth is out of the tip blunting region. The trend of the E and H values with FIB currents is similar to that of the Raman parameters; a minimum is observed around 3-5 nA.

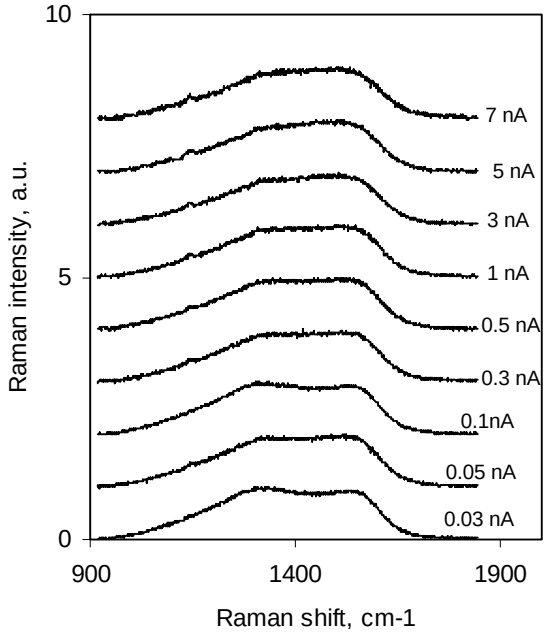

Figure 6: Raman spectra of the IBD samples.

The E and H curves of the thinner EBD films were analysed using an analytical equation adapted from that of Bhattacharya taking into account tip blunting. This recently developed model, which will be published shortly, extract the film's intrinsic hardness and Young modulus values, H_F and E_F. These H_F and E_F values for the 1kV, 2kV and 5kV EBD films are, respectively, 12.9 GPa±1 GPa and 109 GPa±10 GPa, 12.7 GPa±1 GPa and 95 GPa±10 GPa and 12.7 GPa±1 GPa and 100 GPa±10 GPa.

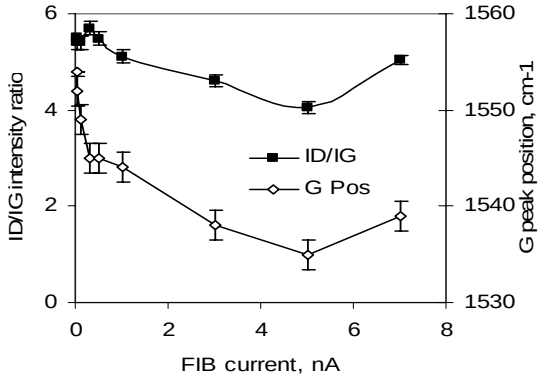

Figure 7: Raman intensity ratio (I_D/I_G) and G peak position (G pos.) for the EBD samples.

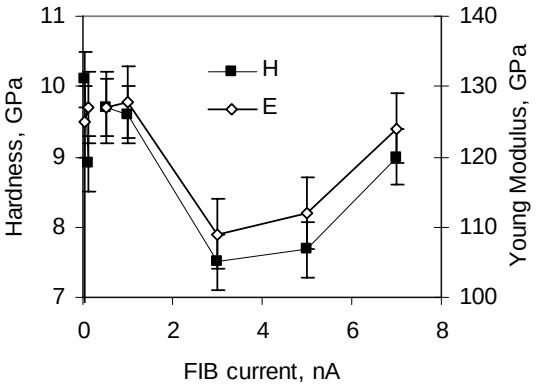

Figure 8: E and H values for the IBD samples at 10% of the film's thickness (50-60nm depth)

4 DISCUSSION

Previous studies on EBD carbon films[11] have also shown that low accelerating voltages give higher growth rate and this is believed to be due to the decreasing secondary electron yield at higher voltages.[12] In addition, despite being exposed to higher charge doses, the EBD samples display smaller growth rates. Ohya[13] has presented comprehensive Monte Carlo simulations of the ion and electron irradiations of solids. According to this study, the generation of secondary electrons in Si is more efficient with the electron beam than with the ion beam whereas in carbon, more secondary electrons are emitted by the ion beam. As most of the growth is taking place on a carbon surface, this may explain the higher IBD growth rates.

The EDX data indicates large Ga atomic percentages. The Kanaya range for 5kV electrons is around 500nm,[14] hence

most of the X-rays are coming from the carbon film. Again, according to Monte Carlo simulations,[13] the Ga^+ ion penetrate about 10-15nm into an aluminium target. As Si and Al have similar atomic number, we also expect the Ga to be contained within a thin surface layer.

The broad and asymmetric Raman features observed in this study are indicative of amorphous carbon, probably hydrogenated, considering the naphthalene precursor and previous results,[7,8] although the luminescence slope, indicative of hydrogen is difficult to notice with 633nm laser excitation. The measured E and H values suggest that these films are somewhat softer than a-C:H films prepared by conventional plasma deposition techniques, although they are much harder than purely graphitic materials such as glassy carbon and graphite. The Raman analysis of the EBD films suggests that, as the kV increases from 1kV to 5kV, these films become less graphitic. This has been observed by others.[11] Figure 5 and 6 indicate that there are more and/or larger sp^2 clusters in the IBD samples. Indeed, FIB irradiation is known to increase the sp^2 fraction of tetrahedral amorphous carbon[15] and, as EBID has been used to form ultrathin electrochemical resist,[7] it is probable that the EBD material has some sp^3 content. However, in these hydrogenated amorphous carbon (a-C:H) films an increase in sp^3 fraction does not necessarily correspond to a mechanical strengthening of the carbon network. The Raman analysis of the IBD samples indicates that, as the FIB current increases, the sp^2 content passes through a minimum, which also correspond to a minimum of the E and H values. Studies of a-C:H films prepared by conventional plasma techniques show that dehydrogenation, and hardening can be associated with an increase in the concentration of carbon double bonds.[16,17] In the case of these IBD samples, it may be that the implanted Gallium further densifies and strengthen the carbon layer.

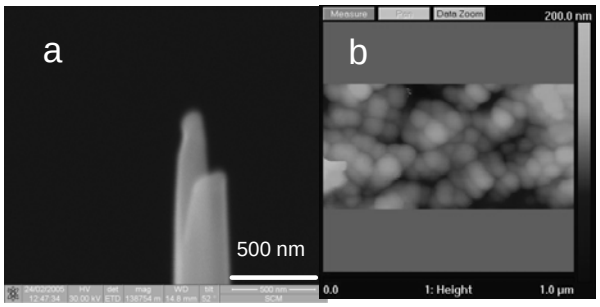

Figure 9: SEM image of the IBD carbon AFM supertip (a) and corresponding 1µm scan TAFM image (b) of a sintered ceramic sample.

These results were used to produce tough AFM supertip carbon structures. These were prepared in spot analysis mode with a two stage FIB process, first with a 10pA, then with 1pA. The resulting supertip, shown in figures 9a has a large base, grown at 10pA current. It culminates in a sharper supertip needle, grown at 1pA, with a sub-100nm end diameter. EDX analysis carried at 5kV with low beam current and high spatial resolution shows that this carbon nanostructure shows a spectrum similar to those presented in figure 4; the needle's composition is essentially C and Ga, with trace quantities of O. Figure 9b shows a tapping mode AFM image of a sintered ceramic obtained with this modified AFM tip. SEM micrographs of the AFM tip after prolonged AFM imaging periods (1 hour) show that the carbon needle structure stayed intact.

4 CONCLUSION

We have prepared EBD and IBD carbon films using a dual FIB/SEM system and analysed their properties by AFM, EDX, Raman and nanoindentation analysis. The films are hydrogenated amorphous carbon. When compared to the EBD films, the IBD samples are Ga implanted, show faster growth rates and larger graphitic content. This study permitted to form carbon AFM supertips which were subsequently used for tapping mode AFM imaging.

REFERENCES

[1] Y.R Cho, Y.R, Lee, Y.H. Song, S.Y. Kang, C.S. Hwang, M.Y. Jung, D.H.Kim, S.K. Lee, H.S. Uhm and K.I. Cho, Mat. Sci. Eng. B, 79, 128, 2001

[2] R.W. Lamberton, S.M. Morley, P.D. Maguire and J.A. McLaughlin, Thin Solid Films, 333, 114, 1998

[3] N.A.Marks, J.M. Bell, G.K. Pearce, D.R. McKenzie and M.M.M. Bilek, Diam. Rel. Mat., 12, 2003, 2003

[4] J. Taniguch, I. Miyamoto, N. Ohno and S. Honda, Nucl. Insts. Meth. Phys. Res. B, 121, 507, 1997

[5] M. Komuro and H. Hiroshima, Microelec. Eng., 35, 273, 1997

[6] M. Castagne, M. Benfedda, S. Lahimer, P. Falgayrettes and J.P. Fillard, Ultramicroscopy, 76, 187, 1999

[7] T. Djenizian, L. Santinacci, H.Hildebrand P.Schmuki, Surface Science 524, 40, 2003

[8] P. Lemoine, J.P. Quinn, P. P. Papakonstantinou, P.D. Maguire and J.A. McLaughlin, Improved carbon materials for nano-manufacturing applications, CRC handbook of nanomanufacturing, Taylor and Francis, 2006

[9] W.C. Oliver, G.M. Pharr, J Mater Res, 7, 1564, 1992

[10] A.K. Bhattacharya and W.D. Nix, Inj. J. Sol. Struct., 24(12), 1287, 1988

[11] W. Ding, D.A. Dikin, X. Chen, R.D. Piner, R.S. Ruoff, E. Zussman, X. Wang and X. Li, J. Appl. Phys., 98, 14905, 2005

[12] M. Amman, J.W. Sleight, D.R. Lombardi, R.E. Welser, M.R. Despande, M.A. Reed and L.J. Guido, J. Vac. Sci. Technol. B, 14(1), 54, 1996

[13] K Ohya and T. Ishitani, Nucl. Inst. Meth. Phys. Res.B, 202, 305, 2003

[14] P. Lemoine, R.W. Lamberton, A.A. Ogwu, J.F. Zhao, P. Maguire and J. McLaughlin, J. Appl. Phys., 86(11), 6564, 1999

[15] A. Stanishevsky and L. Khriachtchev, J. Appl. Phys., 86(12), 7052, 1999

[16] W. Jakob, Thin Solid Films, 326,1, 1998

[17] P. Lemoine, J.P.Quinn, P.D. Maguire, P.P. Papakonstantinou and N. Dougan, Thin Solid Films, on-line proof, 2006